ENGINEERING TRANSACTIONS • *Engng. Trans.* • **60**, 1, 31–39, 2012
Polish Academy of Sciences • Institute of Fundamental Technological Research (IPPT PAN)
National Engineering School of Metz (ENIM)
SIXTY YEARS OF THE ENGINEERING TRANSACTIONS

Analysis of the Cutting Parameters Influence During Machining Aluminium Alloy A2024-T351 with Uncoated Carbide Inserts

Badis HADDAG[1)], Samir ATLATI[1),2)], Mohammed NOUARI[1)], Claude BARLIER[1)], Mohammed ZENASNI[2)]

[1)] *LEMTA CNRS-UMR 7563 – InSIC*
Laboratory of Energetics and Theoretical and Applied Mechanics
27 rue d'Hellieule, 88100 St-Dié-des-Vosges, France
e-mail: badis.haddag@insic.fr

[2)] *EMCS-ENSAO, Mohamed I University*
Team of Mechanics and Scientific Calculations
Oujda, Maroco

This work aims to analyze the effect of the cutting parameters on chip segmentation of the aluminium alloy A2024-T351 during machining process. In this work, two parameters are considered: the tool rake angle of the cutting tool and the feed under dry machining. An orthogonal cutting FE model is developed in Abaqus/Explicit for this purpose. A thermo-visco-plastic-damage model for the machined material and thermo-rigid behaviour for the cutting tool have been assumed. At the chip/tool contact zone, the modified Coulomb friction model has been adopted. Thermal effects are considered by taking into account the heat flux generated by visco-plastic strain and also by friction at the tool-workpiece interface. The obtained results showed the effect of the tool rake angle and feed on the cutting force and chip morphology as well as temperature distribution at the tool rake face.

Key words: orthogonal cutting, tool rake angle, feed, FE analysis, cutting force, chip segmentation.

1. Introduction

Machining processes are widely used in industry to produce parts with complex shapes. An accurate modelling of cutting operations requires consideration of several interacting factors and remains a challenge in industry. Behaviour and numerical aspects should be well considered to obtain accurate results which can be exploited later in an optimisation procedure. To generate a chip in machining, particularly segmented chip, modelling should include a suitable behaviour

law for the workpiece and cutting tool, taking into account work-hardening, strain-rate and temperature effects [2], and adequate contact behaviour at the workpiece-tool interface. A thermo-mechanical coupling should be considered, like the evolution of the heat generated by inelastic strain in the workpiece material and by friction between the chip and tool [3].

To analyse the chip formation process in machining several studies have been carried out following the analytical approach (e.g., [7, 8]). With the development of numerical methods and computation codes simulation of more realistic machining case became possible. The Finite Element (FE) method is widely used for this purpose [3]. Recently, the Smoothed Particle Hydrodynamics (SPH) method has been also applied to analyse cutting processes [4]. In the present paper, an orthogonal cutting operation has been analysed by FE simulations, using Abaqus/Explicit software [1], to analyse both the tool rake angle and feed rate effects on the cutting force, chip morphology as well as temperature distribution at the tool rake face during machining aluminium alloy A2024-T351 with uncoated carbide inserts.

2. Modelling considerations

Since the machining involves intense thermo-mechanical phenomena, each material point in the cutting tool and the workpiece should satisfy simultaneously two equilibrium equations:

$$\text{div}\sigma + f_v = \rho\ddot{u} \qquad \text{and} \qquad k\nabla^2 T - \rho c_p \dot{T} + \dot{q} = 0, \tag{2.1}$$

where σ is the Cauchy stress tensor, f_v is the body forces, $\ddot{u}$ is the acceleration, T is the temperature, ρ is the material density, k is the thermal conductivity, c_p is the thermal capacity, and $\dot{q}$ is the heat source. These equations are strongly nonlinear and coupled, since the stress σ depends on the temperature T via the material behaviour law, as it can be seen in the relationships (2.2)–(2.3). Also, a part of the mechanical inelastic work is to transform to heat, so a part of the heat flux $\dot{q}$ is a function of the flow stress and plastic strain (see Eq. (2.5)). Moreover, in the contact zone a part of $\dot{q}$ is generated by the friction process (see Eq. (2.7)). The heat flux can then be written as $\dot{q} = \dot{q}_p + \dot{q}_f$, where $\dot{q}_p$ and $\dot{q}_f$ are the heat fluxes due to inelastic and friction work, respectively.

2.1. Constitutive model

To represent the behaviour of the workpiece material during machining a Johnson-Cook visco-plastic-damage model has been adopted. The flow stress is given by the following constitutive equation:

$$\overline{\sigma} = \left[A + B(\overline{\varepsilon}^p)^n\right]\left[1 + C\ln(\dot{\overline{\varepsilon}}^p/\dot{\overline{\varepsilon}}_0)\right]\left[1 - ((T - T_0)/(T_m - T_0))^m\right], \tag{2.2}$$

where A, B, C, m, and n are the material parameters, $\overline{\varepsilon}^p$ is the Von Mises equivalent plastic strain, $\dot{\overline{\varepsilon}}^p$ is the strain rate, $\dot{\varepsilon}_0$ is the reference equivalent plastic strain rate, T_m and T_0 are, respectively, the material melting and reference ambient temperatures. The fracture behaviour is described by a damage initiation criterion and a damage evolution law up to fracture. The damage initiation criterion is given by:

$$\omega_d = \int \frac{d\overline{\varepsilon}^p}{\overline{\varepsilon}_d^p} \qquad \text{with} \qquad 0 \leq \omega_d \leq 1 \qquad \text{and}$$
$$\overline{\varepsilon}_d^p = [d_1 + d_2 \exp(d_3 P/\overline{\sigma})] \left[1 + d_4 \ln \dot{\overline{\varepsilon}}^*\right] [1 - d_5 T^*], \tag{2.3}$$

where $\overline{\varepsilon}_d^p$ is the equivalent strain at the onset of damage, function of the stress triaxiality, plastic strain rate, and temperature, while $d_1, ..., d_5$ are the material damage parameters. The criterion for damage initiation is met when $\omega_d = 1$. The true stress evolution after damage initiation ($\omega_d = 1$) and the damage evolution are given by:

$$\widetilde{\sigma} = (1 - d)\overline{\sigma} \qquad \text{with} \qquad d = \overline{u}^p/\overline{u}_f = L\overline{\varepsilon}^p/\overline{u}_f, \tag{2.4}$$

where $\overline{u}^p$ is the equivalent plastic displacement and $\overline{u}_f$ is the equivalent plastic displacement at failure, which is a function of the equivalent plastic strain $\overline{\varepsilon}^p$ and the characteristic length L of the corresponding finite element. This law is introduced to avoid the mesh dependency during damage at the FE scale [1].

As the mechanical behaviour is affected by temperature, the mechanical plastic work generates a heat flux, which results in a temperature rise. The heat flux due to this phenomenon is described by:

$$\dot{q}_p = \eta_p \sigma : \dot{\varepsilon}_p, \tag{2.5}$$

where η_p is the plastic work conversion factor, generally taken equal to 0.9 for metals.

2.2. Tool-workpiece interface behaviour

The contact behaviour at the tool-workpiece interface is defined by the relationship between the normal friction stress σ_n and the shear friction stress τ_f:

$$\tau_f = \min(\mu\sigma_n, \tau_{\max}), \tag{2.6}$$

where μ is the friction coefficient and $\tau_{\max}$ is the shear stress limit considered generally equal to the initial plastic flow shear stress. The friction heat flux at the contact interface is given by:

$$\dot{q}_f = f_f \eta_f \tau_f \dot{\gamma}, \tag{2.7}$$

where $\dot{\gamma}$ is the sliding velocity, τ_f is the friction stress (Eq. (2.6)), η_f is the frictional work conversion factor (η_f is assumed as equal 1), and f_f is the fraction of the thermal energy conducted into the chip. The value of f_f depends on the thermal properties of the cutting tool and workpiece materials, as well as the temperature gradient near the chip-tool interface [3] (f_f is assumed as equal 0.9).

3. Problem description

The problem of the orthogonal cutting test is simulated, with the cutting conditions given Table 1. The corresponding experimental tests are taken from [5]. The experimental setup used to perform the tests is shown in Fig. 1.

Table 1. Cutting conditions: variation of feed and tool rake angle.

Cutting speed V_C [m/min]	Width of cut w [mm]	Feed f [mm]	Tool rake angle α [°]
60	4	0.05, 0.1, 0.3	0, 15, 30

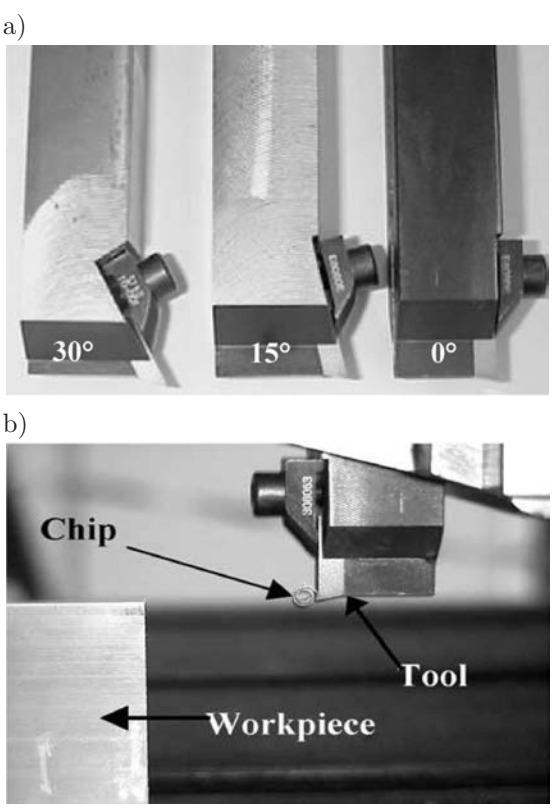

Fig. 1. Experimental setup used for the numerical analysis [5]: a) tool geometry with different tool rake angles, b) orthogonal cutting device.

Geometrical characteristics of the cutting tool and workpiece are given in Fig. 2. Basic physical properties of the workpiece and tool materials are given in Table 2 and behaviour parameters of the workpiece material are given in Table 3.

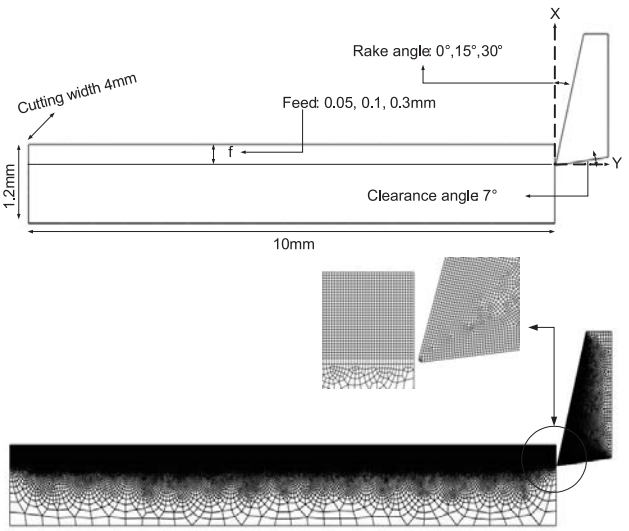

FIG. 2. Geometrical characteristics and mesh of the model.

Table 2. Basic thermo-mechanical properties of the machined workpiece and cutting tool [6].

Physical parameter	Workpiece (A2024-T351)	Tool (WC)
Density, ρ [kg/m^3]	2700	11900
Elastic modulus, E [GPa]	73	534
Poisson's ratio, ν	0.33	0.22
Specific heat, Cp [J/kg/°C]	$Cp = 0.557T + 877.6$	400
Thermal conductivity, λ [W/m/C]	$25 \leq T \leq 300 : \lambda = 0.247T + 114.4$ $300 \leq T \leq Tm : \lambda = 0.125T + 226$	50
Thermal expansion, α [µm·m/°C]	$\alpha = 8.9 \times 10^{-3}T + 22.2$	×
T_m [°C]	520	×
T_0 [°C]	25	25

Table 3. Johnson-Cook parameters of the machined workpiece [6].

Visco-plastic parameters					Damage parameters					
A [MPa]	B [MPa]	n	C	m	$d1$	$d2$	$d3$	$d4$	$d5$	$\overline{u}_f$ [mm]
352	440	0.42	0.0083	1	0.13	0.13	1.5	0.011	0	0.02

4. Results and analysis

4.1. Chip morphology

Several numerical simulations have been performed; some of them are illustrated by Fig. 3. The comparison between the numerical and experimental results shows the direct influence of the cutting parameters on the chip morphology and the temperature distribution at the tool-chip interface. From simulations, the chip thickness and its curvature are dependent on the feed rate as well as on the tool rake angle. This point has been confirmed by experiments. For small feeds ($f = 0.05$ and 0.1 mm), the simulation confirmed the continuous shape of chips, while for large feeds ($f = 0.3$ mm), the chip segmentation is well produced compared to experimental tests. Segmentation intensity is more pronounced for high feeds and small rake angles. The segmentation process is due to the strain localisation in adiabatic shear bands where the thermal softening dominates inducing a decrease of the yield stress inside the bands.

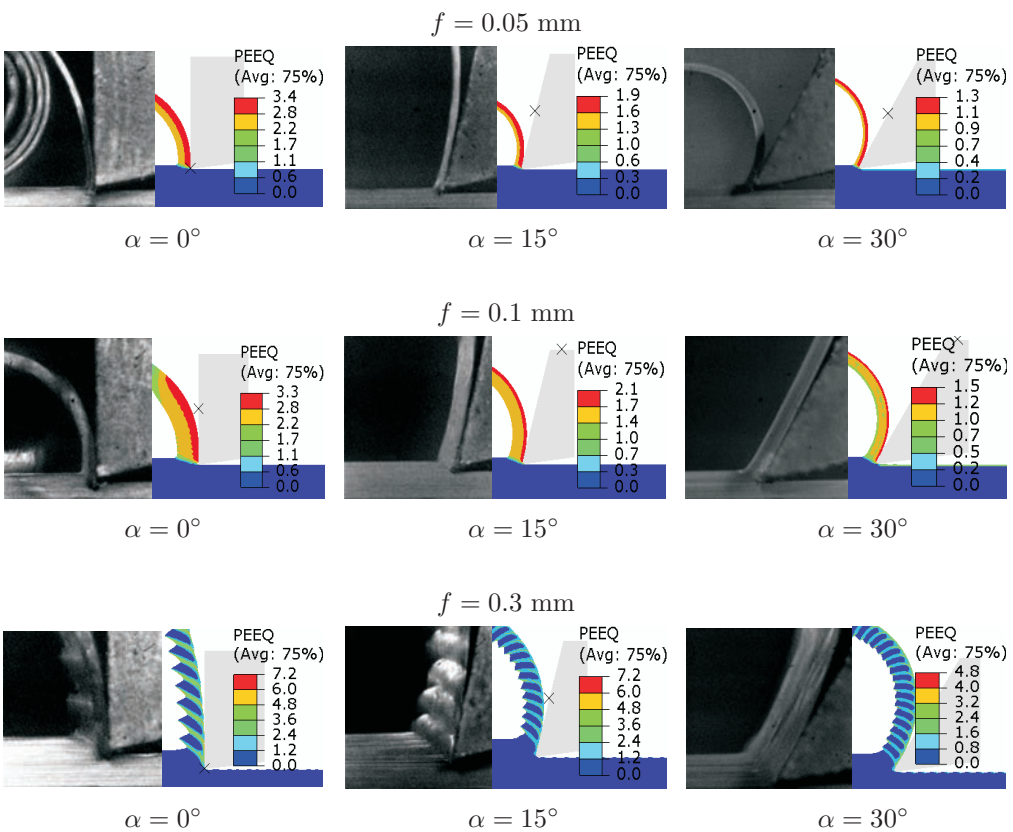

Fig. 3. Comparison between the morphology of the experimental and numerical chips.

4.2. Compression ratio and cutting forces

Variation of the cutting forces with the feed and tool rake angle at a constant cutting velocity is summarized in Fig. 4a. One can observe an increase in the cutting force vs. the feed rate and a decrease vs. the tool-rake angle.

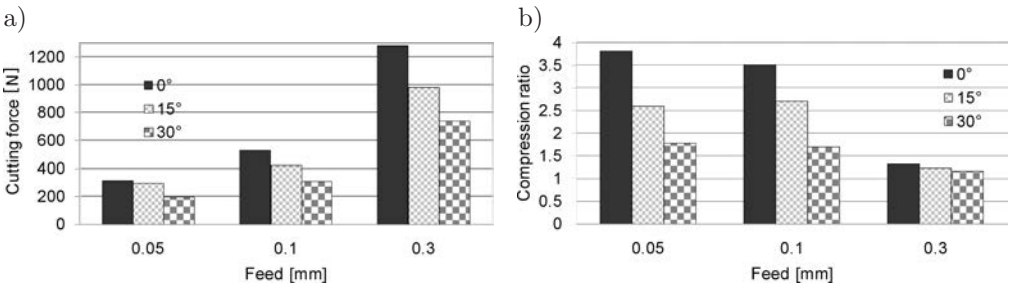

FIG. 4. Cutting force and compression ratio as a function of the tool rake angle and feed.

Variation of the compression ratio, defined as a ratio between the chip thickness and feed, decreases with both feed rate and tool rake angle, as shown in Fig. 4b. A high value is obtained for the small feed and tool rake angle ($f = 0.05$ mm and $\alpha = 0°$), while the small one corresponds to the high feed and tool rake angle ($f = 0.3$ mm and $\alpha = 30°$).

4.3. Tool-chip interface temperature

As shown in Fig. 5, the tool-chip interface temperature increases with the feed ($f = 0.05$, 0.1, and 0.3 mm) and decreases with the tool rake angle ($\alpha = 0$, 15, and 30°). For the high feed (0.3 mm) and high rake angles (30°), the maximum temperature is about 250°C, while for the smallest one, i.e., for the feed (0.05 mm) and tool rake angle (0°), about 150°C is obtained.

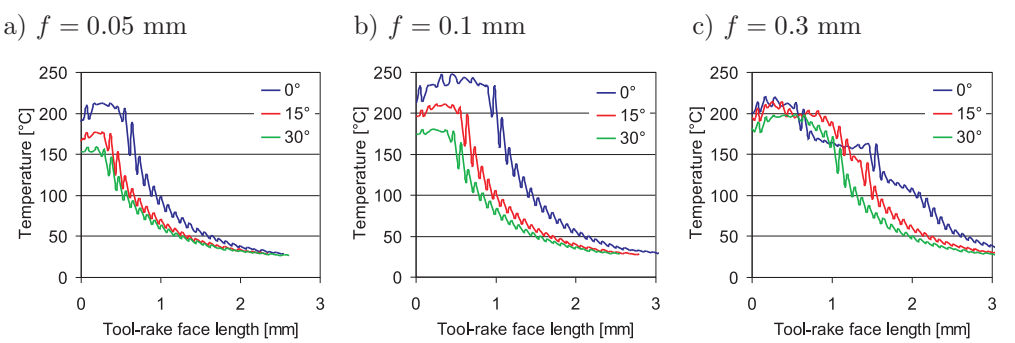

FIG. 5. Tool-rake face temperature distribution at the same cutting length.

The decrease in the temperature level with the rake angle can be explained by the fact that during machining of metallic materials, when the rake angle is large enough, the material flow occurs under sliding contact and with low plastic deformation at the secondary shear zone. Then the produced heat during the chip formation process is lower for the large angles than for the smallest one.

5. Conclusions

The numerical analysis of the cutting process shows in this study the impact of two cutting parameters on some important factors such as the chip morphology, cutting forces, temperature, and compression ratio. The main obtained results can be summarized as follows:

1. For small feeds ($f = 0.05$ and 0.1 mm), the chip has a continuous shape, while for high feeds ($f = 0.3$ mm) it exhibits a segmented shape. However, the numerical simulation for the segmentation process has to be improved, since for $f = 0.3$ mm and $\alpha = 30^\circ$ a continuous shape is shown by experimental tests.
2. Cutting forces show an increase function vs. the feed rate and a decrease function vs. the tool rake angle. It has also been shown in numerical simulations that oscillations in the cutting force curve are obtained when the segmentation occurs.
3. The compression ratio is inversely proportional to both the feed rate and tool rake angle. With this parameter the plastic deformation intensity can be estimated in the chip.
4. One important result from this work concerns the evolution of the cutting temperature with cutting parameters. The numerical results confirm that the tool-chip temperature can be strongly controlled by the tool geometry and feed.

In a future work, chip segmentation prediction will be improved by introducing an adequate damage behaviour for the workpiece material. Simulations with a high cutting speed (HSM) will be performed to highlight its impact on the chip morphology and cutting force reduction.

References

1. ABAQUS Documentation for version 6.8. Dassault Systems Simulia, 2008.

2. Johnson G.R., Cook W.H., *Fracture characteristics of three metals subjected to various strains, strain rates, temperatures and pressures*, Engineering Fracture Mechanics, **21**, 31–48, 1985.

3. Li K., Gao X.-L., Sutherland J.W., *Finite element simulations of the orthogonal metal cutting process for qualitative understanding of the effects of crater wear on the chip formation process*, Journal of Materials Processing Technology, **127**, 309–324, 2002.

4. Limido J., Espinosa C., Salaün M., Lacome J.L., *SPH method applied to high speed cutting modelling*, International Journal of Mechanical Sciences, **49**, 898-908, 2007.

5. List G., Nouari M., Géhin D., Gomez S., Manaud J.P., Le Petitcoprs Y., Girot F., *Wear behaviour of cemented carbide tools dry machining of aluminium alloy*, Wear, **259**, 1177–1189, 2005.

6. Mebrouki T., Girardin F., Asad M., Rigal J-F., *Numerical and experimental study of dry cutting for an aeronautic aluminium alloy (A2024-T351)*, International Journal of Machine Tools and Manufacture, **48**, 1187–1197, 2008.

7. Molinari A., Moufki A., *The Merchant's model of orthogonal cutting revisited: A new insight into the modelling of chip formation*, International Journal of Mechanical Sciences, **50**, 124–131, 2008.

8. Ozlu E., Budak E., Molinari A., *Analytical and experimental investigation of rake contact and friction behaviour in metal cutting*, International Journal of Machine Tools and Manufacture, **49**, 865–875, 2009.

Received May 10, 2011; revised version August 23, 2011.